SCIENCE CHINA
Earth Sciences

•RESEARCH PAPER•

August 2020 Vol.63 No.8: 1209–1222
https://doi.org/10.1007/s11430-018-9385-3

The comparison of statistical features and synoptic circulations between the eastward-propagating and quasi-stationary MCSs during the warm season around the second-step terrain along the middle reaches of the Yangtze River

Ruyi YANG[1,2], Yuanchun ZHANG[1*], Jianhua SUN[1,2] & Jun LI[3]

[1] *Institute of Atmospheric Physics, Chinese Academy of Sciences, Beijing 100029, China;*
[2] *University of the Chinese Academy of Sciences, Beijing 100049, China;*
[3] *31010 PLA Troops, Beijing 100081, China*

Received March 9, 2018; revised March 4, 2019; accepted June 18, 2019; published online June 4, 2020

Abstract Mesoscale convective systems (MCSs) around the second-step terrain (106°–113°E, 28°–35°N), along the middle reaches of the Yangtze River, were detected, tracked and classified using a black body temperature (TBB) dataset during May to August 2000–2016 (except 2005). The MCSs were divided into eastward-propagating (EP) and quasi-stationary (QS) types, to compare their spatial and temporal distributions and convective intensities, and to identify the favorable synoptic conditions for the formation and evolution of EP MCSs. The results showed that both MCS types occurred most often in July. The EP MCSs were mainly initiated over the eastern regions of the study area, while the QS type mainly originated in the western regions of the study area. Both MCS types mainly formed in the afternoon, but a second peak occurred in the early morning for QS MCSs. The EP MCSs had a larger cloud area at their mature stage and a lower cloud brightness temperature, indicating more intense convection. Additionally, the longer lifetime and further eastward propagation of the EP MCSs meant that they had a great influence on the precipitation over the middle and lower reaches of the Yangtze River. Synoptic circulation analysis demonstrated that the combination of the mid-level low trough east of the Tibetan Plateau (TP), and the western pacific subtropical high (WPSH), favored the formation and eastward propagation of EP MCSs. The positive vertical relative vorticity and stronger vertical wind shear provided dynamic conditions favorable for convective organization and development. Furthermore, a stronger low level jet imported warm and moist air to the eastern edge of, and the regions east of, the second-step terrain. The substantial convergence of water vapor promoted the development and long-lived maintenance of the EP MCSs.

Keywords Second-step terrain, Middle reaches of the Yangtze River, Mesoscale convection systems, Spatial and temporal distribution, Synoptic circulation

Citation: Yang R, Zhang Y, Sun J, Li J. 2020. The comparison of statistical features and synoptic circulations between the eastward-propagating and quasi-stationary MCSs during the warm season around the second-step terrain along the middle reaches of the Yangtze River. Science China Earth Sciences, 63: 1209–1222, https://doi.org/10.1007/s11430-018-9385-3

1. Introduction

Mesoscale convective systems (MCSs) are a significant weather system in the occurrence and evolution of severe weather, including heavy rainfall, lightning and hail (Maddox, 1980; Tollerud and Collander, 1993; Houze, 2004; Zheng et al., 2013). In recent decades, improvements in satellite remote sensing and radar detection have enabled high spatial and temporal resolution datasets to be applied to explore the spatial and temporal distribution of MCSs over various regions; particularly important are stationary satellite observation data with longer time series, higher resolution

* Corresponding author (email: zhyc@mail.iap.ac.cn)

and better quality control (Maddox, 1980; Augustine and Howard, 1991; Laing and Fritsch, 1997; Anderson and Arritt, 1998; Jirak et al., 2003; Zheng et al., 2008; Goyens et al., 2012; Zhuo et al., 2012).

Because of its complex terrain distribution, there are regional differences in the spatial and temporal features of MCSs in China (Zheng et al., 2008; Qi and Zheng, 2009). MCSs over the Tibetan Plateau (TP) show clear temporal variations, occurring mainly in the afternoon. However, MCSs over the Sichuan Basin mostly occur during the nighttime and the convection over plains can also be initiated during the afternoon and early morning (Jiang and Fan, 2002; Zheng et al., 2008; Bai et al., 2011; Fu et al., 2013; Hu et al., 2016). The MCSs form during the afternoon to early evening, mature around the early evening and decay or weaken during the nighttime over the plains (including, for example, the lower reaches of the Yellow River, the Yangtze and Huai Rivers and South China), although long-lived MCSs can form earlier (Rowell and Milford, 1993; Mathon and Laurent, 2001). MCSs over the Yangtze-Huai River Valley and the lower reaches of the Yellow River mostly occur in July, but those over South China mainly appear in June (Qi and Zheng, 2009; Zhuo et al., 2012; Li et al., 2015; Liu et al., 2015). MCSs with a larger cold cloud area can be maintained for a longer time (Tollerud et al., 1992; Durkee and Mote, 2010; Rafati and Karimi, 2017); the area and duration are determined by the rate of increase of the cloud area during the early stages (Tollerud et al., 1992; McAnelly and Cotton, 1992) and the merging of convective clusters. Pope et al. (2008) studied MCSs in the northern regions of Australia and their surroundings. They found that the maintenance of short-lived MCSs is related to the initial rate of area increase, while clouds merging is the main factor in the development of long-lived MCSs.

The development and organization of MCSs are impacted by synoptic circulations. Previous studies demonstrate that the environment of MCSs generally features specific dynamic and thermal conditions (Maddox, 1983; Cotton et al., 1989; Sun et al., 2004; Coniglio et al., 2010; Zheng and Sun, 2013; Zheng et al., 2013; Punkka and Bister, 2015; Zeng et al., 2016). A comparison of the synoptic circulations of a mesoscale convective complex (MCC) in null- and active-MCC periods shows that low-level thermal forcing and conditional instability are important for MCS development (Merritt and Fritsch, 1984; Augustine and Howard, 1991). The low-level jet (LLJ) also plays an important role in MCS evolution: firstly, the transportation of warm and moist air at low levels intensifies the instability of atmospheric stratification, which favors MCS initiation; secondly, the convergence and upward motion ahead of the maximum wind speed of the jet provide the abundant water vapor and dynamic conditions necessary for MCS development (Trier and Parsons, 1993; Augustine and Caracena, 1994; Nicolini and Torres Brizuela, 2002; Salio et al., 2007).

The initiation and development of MCSs are different for different underlying surface conditions (Velasco and Fritsch, 1987; Laing and Fritsch, 1997; Zipser et al., 2006; Schröder et al., 2009; Romatschke and Houze, 2010; Rasmussen and Houze, 2011; Rafati and Karimi, 2017; Zheng et al., 2008; Qi and Zheng, 2009). Most previous studies of MCSs in China focused on the Tibetan Plateau and the Yangtze and Huai River Valley, whereas few studies have looked at MCSs on the second-step high terrain, which includes the Taihang Mountains, the Loess Plateau over northern China, the Qinling Mountains over central China and the Yungui Plateau over southwestern China (Figure 1). Recent case studies have shown that severe convective systems mainly appear over the Yangtze-Huai River Valley to the east of the second-step terrain, causing heavy rainfall, lightning, hail, high wind and other hazardous weather (Meng et al., 2013; Zheng et al., 2013; Zheng et al., 2016). These convective systems can be traced back to eastward-propagating convective systems over the second-step terrain (He and Zhang, 2010; Sun and Zhang, 2012; Zhang and Sun, 2017, Zhang et al., 2018). This study identifies and tracks MCSs over the second-step terrain along its middle reaches, and classifies them in order to analyze the background circulations which are favorable for their eastward propagation.

2. Data and method

MCSs over the study region (106°–113°E, 28°–35°N, the purple box in Figure 1) were detected using the hourly black body temperature (TBB) from Japanese satellites (http://weather.is.kochi-u.ac.jp/archive-e.html) between May and August from 2000 to 2016 (except 2005). These satellite data, at 0.05°×0.05° horizontal resolution, included four infrared channels and one visible channel (IR1, IR2, IR3, IR4 and VIS) from the stationary satellites GMS5, GOES-9, MTSAT-2 and Himawari-8 (Table 1). The IR1 record was used in this study. The data for 2005 were not included for analysis because of the large missing rate in this year although, in any case, only 21 MCSs were detected (based on TBB from FY-2C) from May to August in 2005, accounting for a low proportion of the total statistical results. The integrity rate of the data overall was 95.98%; the rate was higher than 90% in each year and the highest rate for a single year was 99.32%. Besides the TBB dataset, six-hourly climate forecast system reanalysis (CFSR) data ($0.5^{o}\times0.5^{o}$) from the National Centers for Environment Prediction (NCEP) were utilized to composite the background circulation. In order to compare the circulations at each stage of the MCSs, the six-hourly CFSR data (at 00, 06, 12, 18 UTC) were interpolated to three-hourly resolution, with values at 00, 03, 06, 09, 12, 15, 18 and 21 UTC. From the Navier-

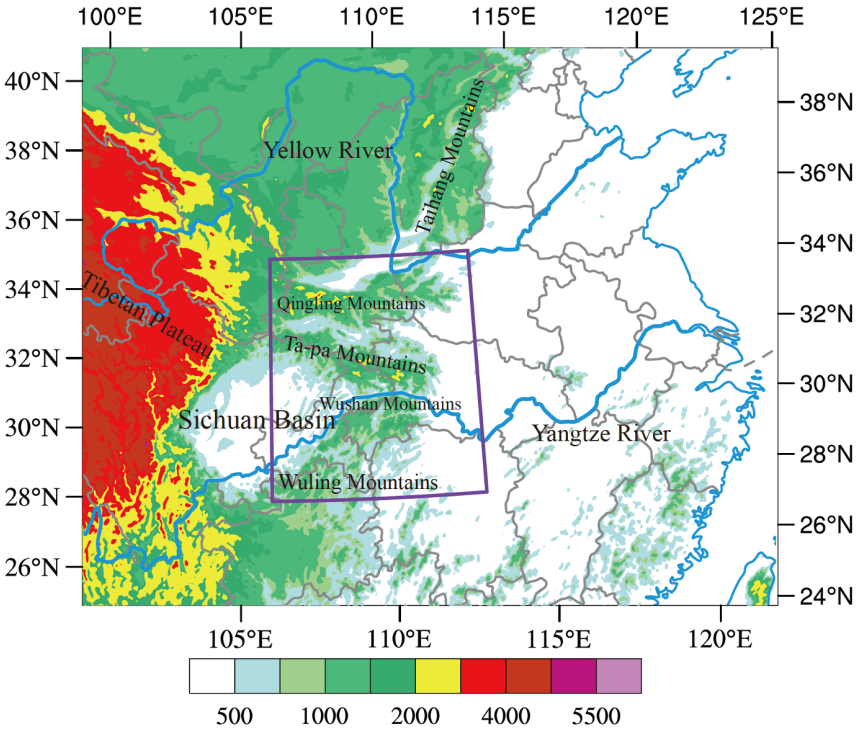

Figure 1 Geographical distribution of elevation in East China (shading, units: m). The purple box denotes the study area.

Table 1 Time periods of satellite data used in this study

Satellite	Time period
GMS5	May 1 2000–May 21 2003
GOE9	May 22 2003–August 31 2004
MTSAT-1R	May 1 2006–August 31 2010
MTSAT-2	May 1 2011–July 6 2015
Himawari-8	July 7 2015–August 31 2016

Stokes equations, the time scale of mesoscale convection should be f^{-1}, the inverse of the Coriolis parameter, which is about 3 hours in the middle latitudes (Parker and Johnson, 2000). Therefore, the three-hourly interpolated CFSR data are appropriate for the composition analysis. All times given in the rest of this manuscript are expressed in Beijing Standard Time (BST).

It has been demonstrated that brightness temperatures obtained from infrared radiance images can be used to detect and track MCSs, a process aided by the strong contrast between the cold cloud tops and the warmer background (Kidder and Vonder Haar, 1995). Maddox (1980) used the criteria TBB ≤−32°C and cloud area ≥10^5 km^2, and TBB ≤−52°C and cloud area ≥5×10^4 km^2, to detect MCCs in the central United States, based on infrared satellite images. Augustine and Howard (1988) found that applying only the second criterion could better describe the evolution of MCCs. This second criterion (TBB ≤−52°C and cloud area ≥5×10^4 km^2) has since been widely applied (Zheng et al., 2008; Durkee and Mote, 2010; Yang et al., 2015). Zheng et al. (2008) also demonstrated that applying the criterion that infrared brightness temperature ≤−52°C could show the spatial and temporal distribution features of MCSs over China and its vicinity. The criterion cloud area ≥5000 km^2 has been used to track the evolution of MCSs throughout their whole lifetimes (Mathon and Laurent, 2001; Tomasini et al., 2006; Ogungbenro et al., 2016). Combing results from previous studies and the cloud cluster features in the present study region (Figure 1), the detection criteria for MCSs over the second-step terrain along the middle reaches of Yangtze River were defined as follows: (1) The area of the MCS contiguous cloud shield (TBB ≤−52°C) should be greater than or equal to 5000 km^2; (2) the duration of the MCS should be greater than or equal to three hours; and (3) the MCS is no longer tracked and considered terminated when its size as defined in condition (1) falls below 5000 km^2 (Table 2).

The method applied to automatically recognize and track MCSs was based on the theory of pattern recognition and matching in the field of digital image processing technology (Li, 2010; Li et al., 2012).This method uses an eight-neighbor contour tracking algorithm to detect the cloud boundary line and to match the feature parameters, such as the distance of two clouds, cloud area change rate, shape descriptor R (Lu et al., 1987) and Hu invariant moments (Hu, 1962), between two neighboring times. While detecting and tracking MCSs, some cloud attributes, such as cloud center, area, cir-

cumference etc., were also calculated. Splitting and merging during the cloud evolution were handled as follows: when a cloud splits, the tracked cloud at the next time is the one that is the most similar to the cloud before splitting; when clouds merge with one another, only the largest of them continues to be tracked at subsequent times. A manual validation was used to improve the results of the automatic detection and tracking. Figure 2 shows the tracks of the total MCSs detected using the criteria in Table 2. If an MCS center at the termination stage is within the study region (106°–113°E, 28°–35°N), that MCS is classified as quasi-stationary (QS). If the MCS center at the termination stage is eastward of 113°E (the eastern edge of the study region, shown in Figure 1), it is classified as eastward-propagating (EP). Besides the EP MCSs, some of the MCSs propagated westward, northward and southward (31 cases, about 4% of the total): these were not included in this study. The statistical features of the QS and EP MCS types will be compared in following sections.

3. The statistical features of eastward-propagating and quasi-stationary MCSs

3.1 The temporal features of the two MCS types

A total of 737 MCSs were detected over the second-step terrain along the middle reaches of the Yangtze River from May to August 2000–2016 (except 2005) and the average annual number was about 46.1. A total of 193 of the 737 MCSs were EP type, accounting for about 26.2%, and the average annual number was 12. 513 of the total cases (about 70%) were QS type, with an average annual number of 32. The maximum number of total MCSs occurred in 2007 and the minimum in 2014 (Figure 3a). The maximum occurrence of EP MCSs was also in 2007 and the minimum is in 2012, while the maximum occurrence of QS MCSs is in 2016 and the minimum in 2014. In most years, EP MCSs occurred less often than QS MCSs (Figure 3a). The monthly variation had a maximum in July and a minimum in May (Figure 3b). Yang et al. (2015) also found that the MCS occurrence over China

Table 2 MCS detection criteria

Definitions	Criterion
Scale	The MCS's contiguous cloud shield (TBB ≤−52°C) should be no less than 5000 km^2
Initiation	The first time that an MCS satisfies the above scale
Maturity	The time when the cloud-shield area of an MCS reaches its maximum
Termination	The first time that an MCS no longer satisfies the above scale
Duration	The duration of the MCS should be no shorter than 3 hours

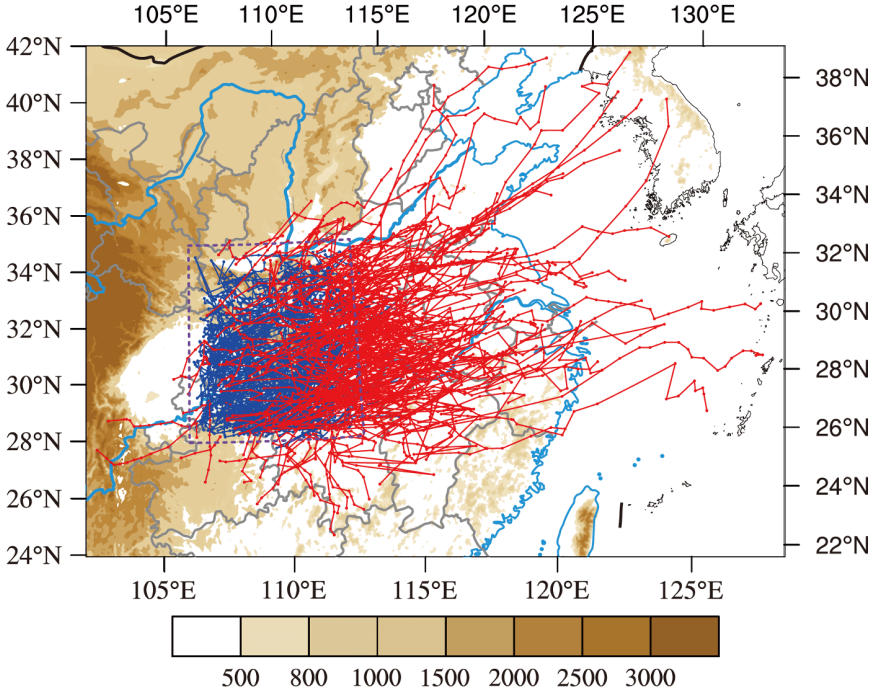

Figure 2 Tracks of all MCSs. Colored shading denotes elevations higher than 500 m (units: m), the purple box denotes the study area. The red solid lines mark trajectories of MCSs propagating out of the study region, with their central locations at each recording time represented by red dots, while the bluelines mark trajectories of quasi-stationary MCSs, with their central locations at each recording time represented by blue dots.

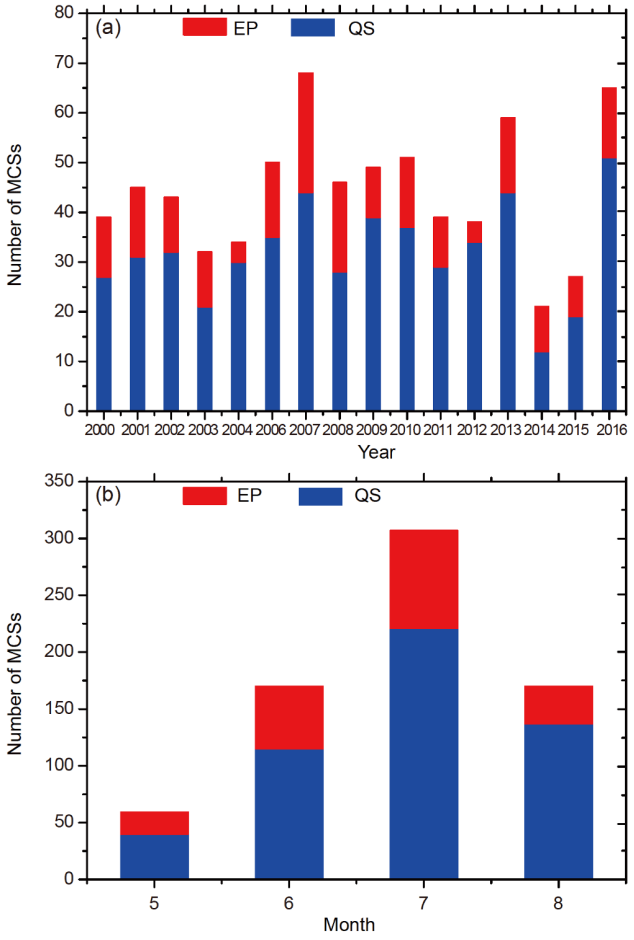

Figure 3 Annual variations (a) and monthly variations (b) of the EP (red) and QS (blue) MCSs.

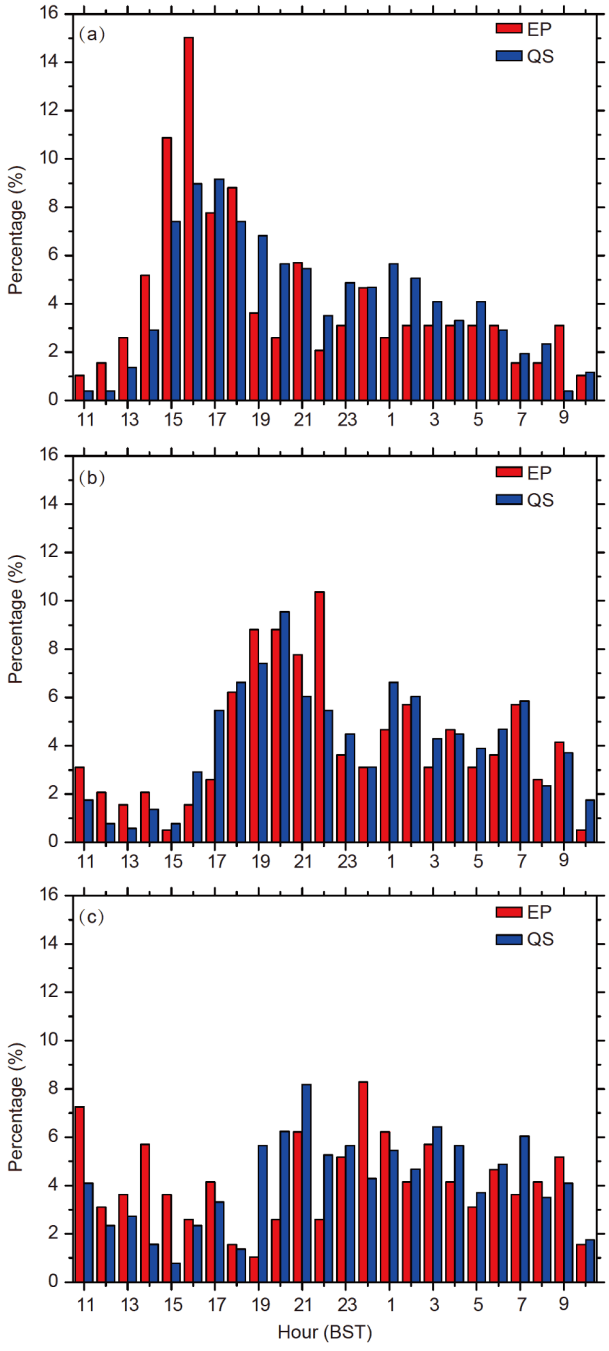

Figure 4 Diurnal variations of the eastward-propagating (red) and quasi-stationary (blue) MCSs: (a) formation, (b) maturity, (c) termination.

and its vicinity peaks in July and has a minimum in May.

In order to further compare the temporal features, the diurnal variations of the two-type MCSs at formation, mature and termination stages are analyzed below. The formation stage is the first time that an MCS satisfies the condition that the contiguous cloud shield (TBB ≤ -52°C) has an area no less than 5000 km^2; the mature stage is the time when the contiguous cloud shield (TBB ≤ -52°C) reaches its maximum area and the termination stage is the first time that the MCS no longer satisfies the first condition. It was found that the occurrence frequencies of MCS formation were different for the two types (Figure 4a). Though both types of MCS formed mainly in the afternoon, the formation of EP MCSs peaked at ~16 BST, and that of QS MCSs had two peaks (one in the afternoon and one in the early morning), but the main peak was at 17 BST. The horizontal distributions of the MCSs at the formation stage illustrated that most of the EP MCSs originated over the eastern edge of the second-step terrain and the transition regions between the second-step terrain and its eastern plains. The QS MCSs mainly formed in the eastern part of Sichuan Basin and mountainous regions in the early morning (Figure 5b), which was consistent with the nocturnal convection in Sichuan Basin (Zheng et al., 2008). Both EP and QS MCSs matured in the early evening and nighttime; the former peaked at 22 BST and the latter at 20 BST (Figure 4b). There was also a second peak in the early morning for both EP and QS MCSs. EP MCSs mainly terminated in the middle reaches of Yangtze River, and some of them propagated eastward to the ocean in the morning and afternoon (Figure 5e). For the QS MCSs (Figure 5f), the termination in the western part of the second-step terrain occurred in the evening and that in the eastern part occurs in the morning.

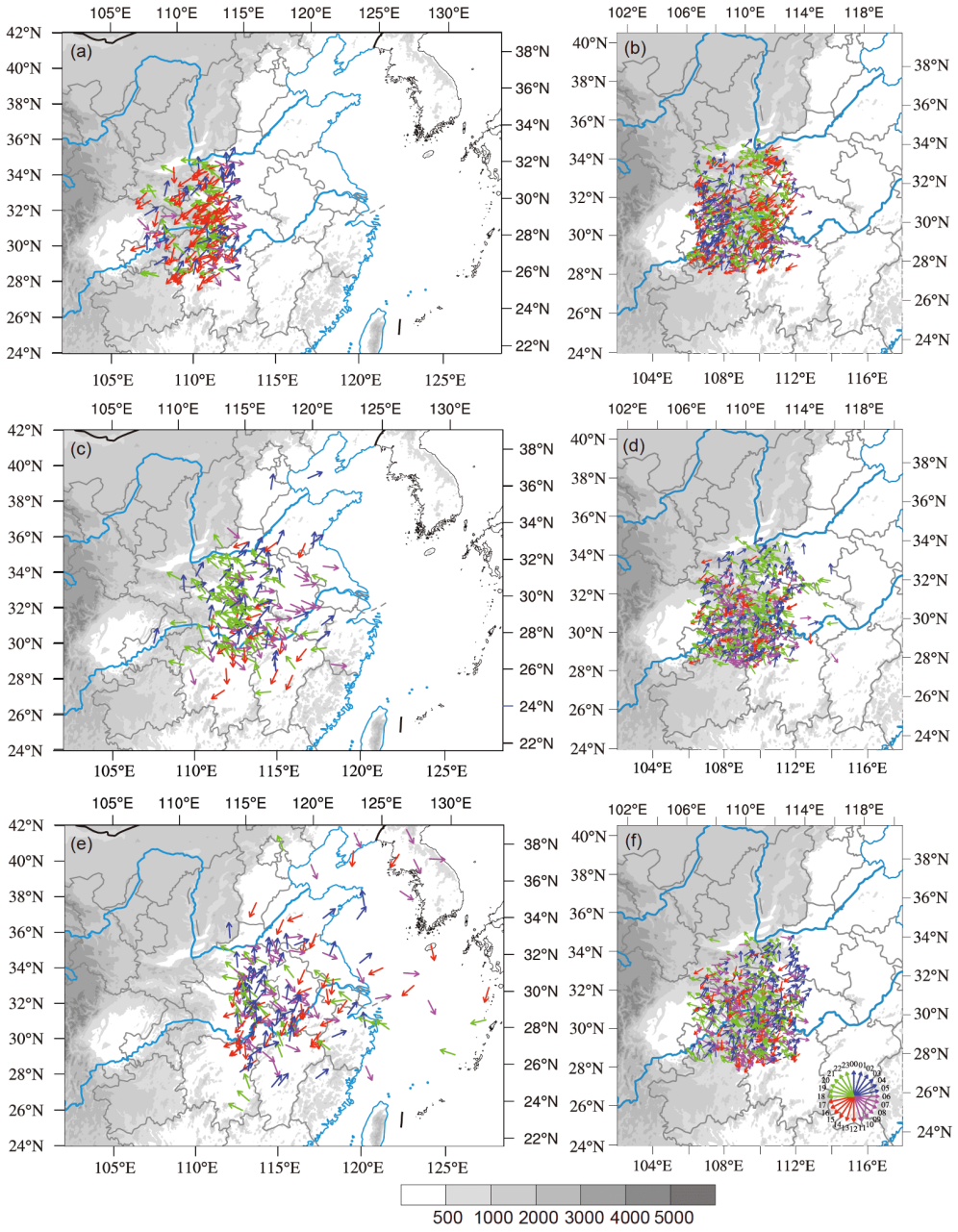

Figure 5 The location and time of the EP and QS MCSs at different stages; the arrows mark the locations and the direction of an arrow denotes the time (BST); the gray shading denotes elevation higher than 500 m (units: m). The panels show EP MCSs: (a) formation, (c) maturity, (e) termination; and QS MCSs: (b) formation, (d) maturity, (f) termination.

EP MCSs formed in the afternoon (15–18 BST), matured in the early evening and at night time (19–22 BST), and terminated in the evening and the following early morning (21–03 BST). The formation and maturity of QS MCSs were earlier than those of EP MCSs; additionally, QS MCSs also terminated earlier, which means that they could take less time to decay.

3.2 Tracks and lifetimes of the two MCS types

Figure 6 shows that, as well as differences in formation, maturity and termination, there were differences in the tracks and lifetimes between the two MCS types. The EP MCSs propagated further eastward and influenced larger areas (Figure 6a), whereas the tracks of QS MCSs remained concentrated in the study region (Figure 6b). Previous studies also found that MCSs in South China mainly propagate eastward (Li et al., 2015) and most of the MCCs north of the Yangtze River move northeastward (Chang and Ding, 2015). Most of the EP MCSs decayed over the central and eastern regions of China and only a few propagated further eastward to the ocean. A few of them (~1.5%)

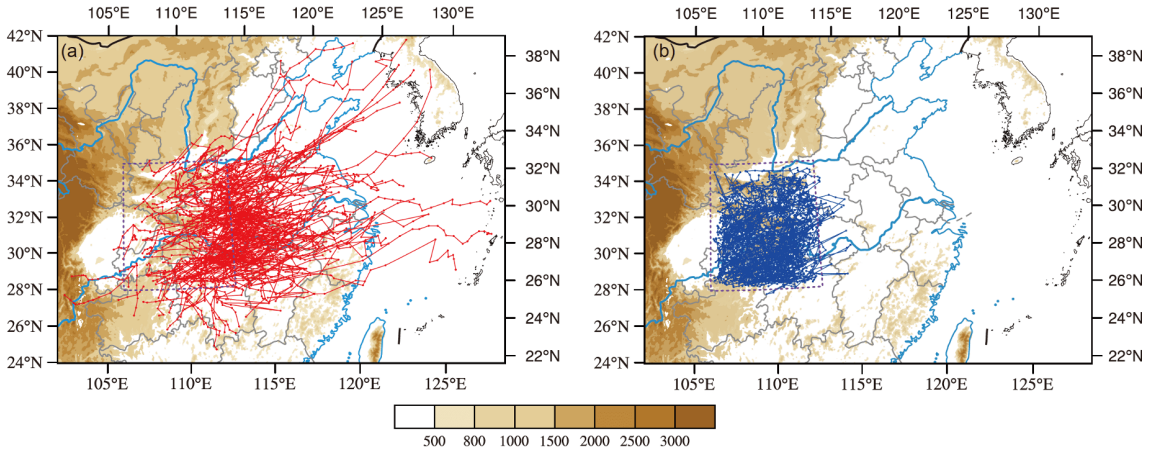

Figure 6 Tracks of EP and QS MCSs. Color shading denotes elevation higher than 500 m (units: m), and the purple box denotes the study region. (a) EP MCSs: the red lines mark trajectories, and the red dots represent the central location at each recording time; (b) QS MCSs: the blue lines mark trajectories, and the blue dots represent the central location at each recording time.

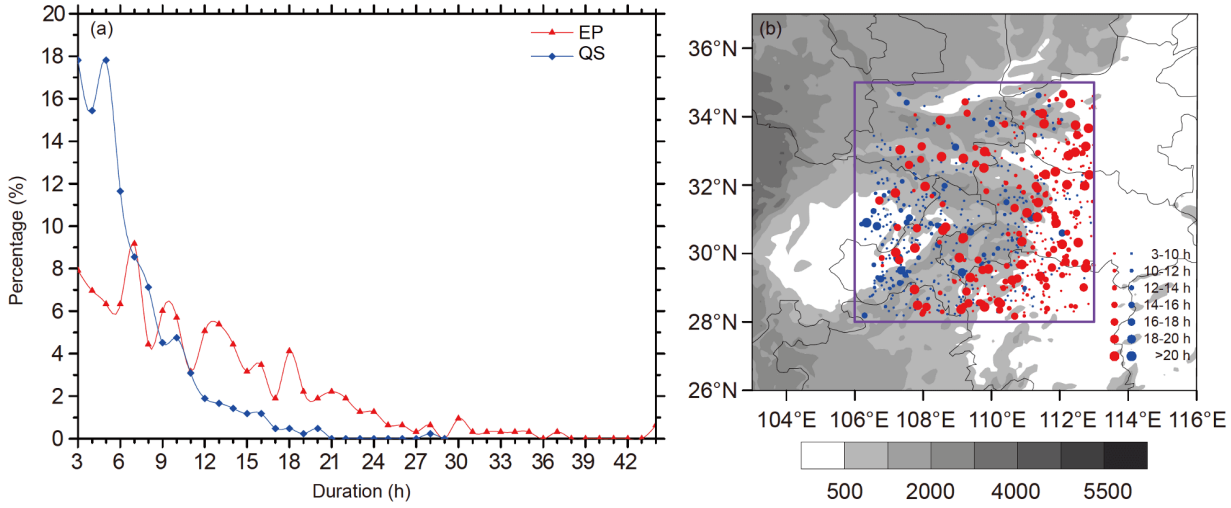

Figure 7 (a) The duration of the EP (red line) and QS (blue line) MCSs. (b) The formation location and duration of the EP (red dots) and QS (blue dots) MCSs: the size of the dots represents the lifetime as shown (unit: hour); gray shading denotes elevation higher than 500 m(units: m), and the purple box denotes the study area.

moved southeastward and had an impact on the southern regions of Hunan and Jiangxi provinces, and about 2.0% of them propagated northeastward to North China with some reaching the Korean Peninsula. The QS MCSs originated in the western region of the second-step terrain (Figure 6b) and most of them developed and terminated within the study region.

The propagation regions of the MCSs were related to their lifetimes (Liu et al., 2015). On the whole, the lifetimes of EP MCSs were longer (Figure 7a). The frequency of occurrence decreased with increasing lifetime for both types, but their frequency distributions were different. The average lifetime of EP MCSs was about 14.2 hours, but that of QS MCSs was only about 6.6 hours, around half of EP value. About 50% of the QS MCSs lasted less than 6 hours and the frequency decreased with increasing lifetime above 6 hours. 23% of the EP MCSs lasted more than 20 hours, and only 10% lasted less than 6 hours, with the frequency peaking at 7 and 9 hours. Looking at the monthly variation, the lifetimes of EP MCSs were longer than those of QS MCSs in each month (Figure 8). For EP MCSs, the frequency of occurrence had a maximum value in May with a large monthly variation. Because the QS MCSs mainly evolved within the study region, the lifetimes in each month were similar. Most of the EP MCSs lasted longer and propagated eastward to the downstream regions, influencing the convective systems in the eastern plains. But some MCSs, with shorter lifetimes, originated in the eastern edge of the second-step terrain and its transition region to the plains.

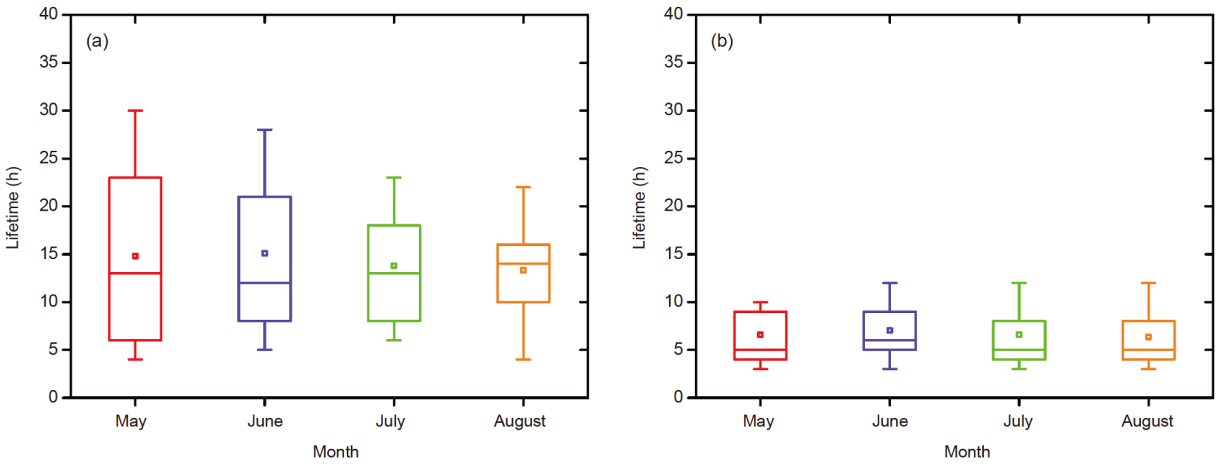

Figure 8 The monthly distribution of lifetimes of the EP (a) and QS (b) MCSs; the box covers the 25th–75th percentiles, the horizontal line in box marks the median value, the square denotes the mean value, and the lower and upper whiskers cover the 10th–90th percentiles.

3.3 Cloud parameters of the two MCS types

In order to better compare the cloud features of the two MCS types, the mature stage was defined as the time at which the area of the cloud reaches its maximum in the whole lifetime and the lowest temperature was defined as the lowest cloud-shield brightness temperature in the MCS lifetime. The cloud-shield area at the MCS mature stage (M-AREA for short) and the lowest brightness temperature (L-TEMP for short) indicated the intensity of an MCS and were related to the convective rainfall (Goyens et al., 2012; Ai et al., 2016). Most of the MCS M-AREAs for both types were larger than 10^4 km^2 (Figure 9a). 36% of the EP MCSs and 75% of the QS MCSs were between 10^4 km^2 and 5×10^4 km^2 in area. The number of QS MCSs decreased with increasing M-AREA larger than 5×10^4 km^2, and there were more EP MCSs with these values (Figure 9a). Moreover, most of the QS MCSs had the M-AREAs less than 2×10^5 km^2, while 8.6% of the EP MCSs reached a cloud area larger than 2×10^5 km^2. The number of MCS occurrences increased and then decreased with increasing L-TEMP, for both MCS types. For EP MCSs, the L-TEMP range which occurred most often was between −80 and −75°C, while for QS cases, the range between −75 and −70°C occurred most often. 62.7% of the EP MCSs and 29.9% of the QS MCSs had an L-TEMP lower than −75°C.

In order to explore the time series of the two parameters defined above, the differences of the times at which the MCSs reached the M-AREA and L-TEMP values were compared in Figure 9c. The time difference between formation and reaching M-AREA (L-TEMP) was defined as DT-AREA (DT-TEMP), indicating the period from MCS formation to mature stage (lowest cloud-shield brightness temperature). As a whole, the numbers of MCSs with DT-AREA and DT-TEMP about 5 hours accounted for more than half of the total MCSs for both types and the time differences in most cases were within the range of 0–4 hours (Figure 9c). Ai et al. (2016) also found that the M-AREA and L-TEMP appear about 5 hours after the MCS formation, when they explored the lifetimes of MCSs in central and eastern China. Compared with the QS MCSs, the DT-AREA and DT-TEMP values for EP MCSs were greater, indicating that the EP MCSs took a longer time from formation to reaching M-AREA (L-TEMP), which was in agreement with their longer lifetimes discussed in subsection 3.2. Additionally, DT-AREA for both MCS types was greater than DT-TEMP, indicating that L-TEMP was reached earlier than M-AREA during the MCS evolution. A possible explanation is that the strong convection of rapid upward motion related to L-TEMP caused heavy rainfall and then was followed by an enlargement of the cloud shields (Hodges and Thorncroft, 1997; Mathon and Laurent, 2001; Pope et al., 2008). L-TEMP for QS MCSs was reached one hour earlier than M-AREA (Figure 9c), meaning that the cloud shield area reaches its maximum one hour after L-TEMP was reached. For the EP MCSs, the differences between DT-TEMP and DT-AREA were about 2 hours, longer than those of the QS MCSs, which means that it took longer for EP MCSs to reach the cloud maximum area. DT-AREA and DT-TEMP were normalized, divided by the whole lifetime, in order to compare the two periods as percentages of MCS lifetime. The results showed that DT-TEMP was reached during the first half of the whole lifetime, and occurred earlier than the mature stage, which mainly appeared halfway through the lifetime (Figure 9d). The times at which EP and QS MCSs reached their mature stages were similar, but the times at which L-TEMP was reached are different (that of the QS MCSs is earlier).

L-TEMP was divided into four ranges in order to explore the relationship between M-AREA and L-TEMP and compare the M-AREAs of the two MCS types (Figure 9e). M-AREA decreased with increasing L-TEMP, especially for the EP MCSs. For all four ranges, the M-AREAs of the EP cases

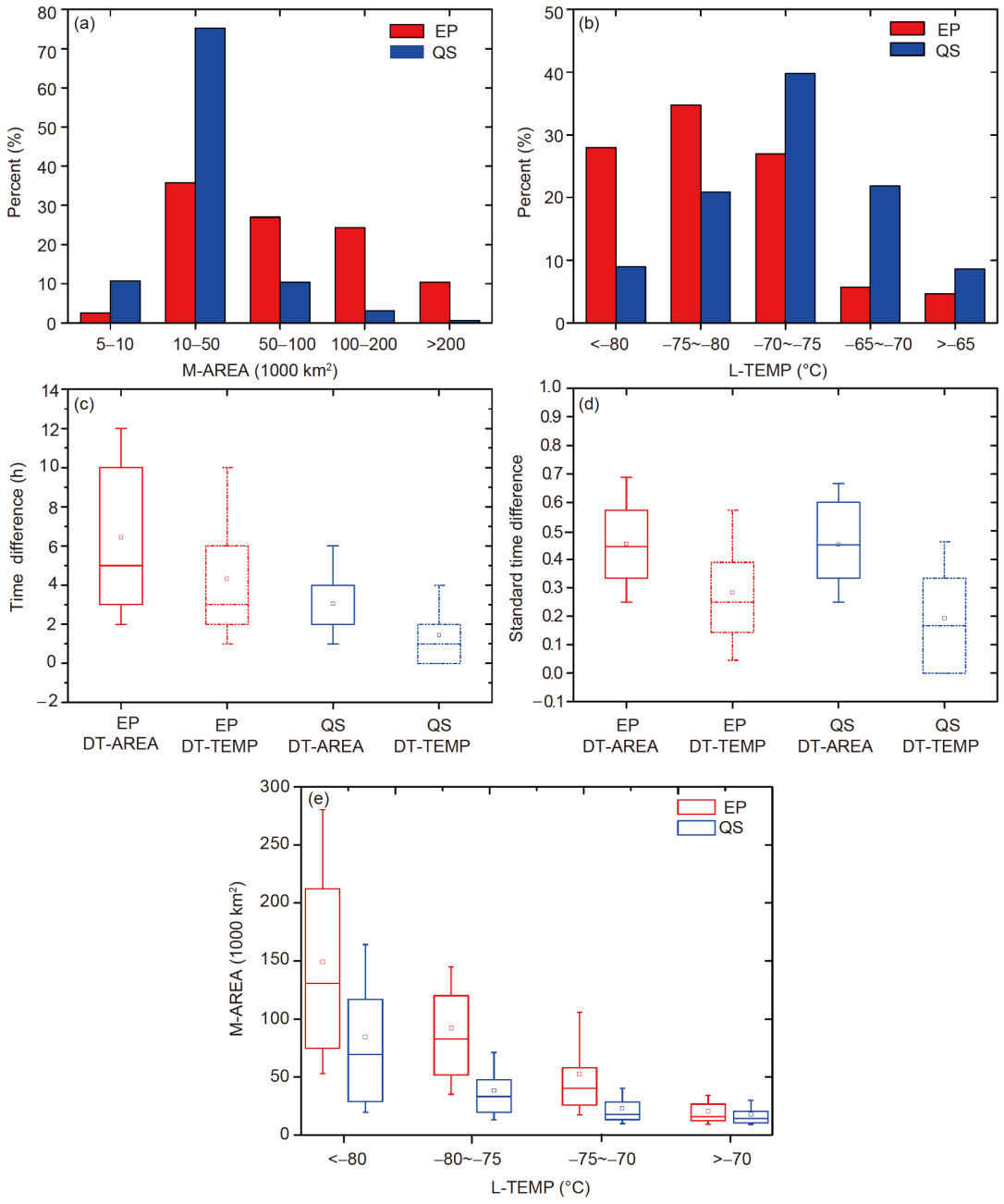

Figure 9 The cloud parameters of the EP (red) and QS (blue) MCSs; the solid lines indicate maximum area, the dotted lines represent minimum temperature: (a) percentage of MCSs within different maximum area ranges, (b) percentage of MCSs within different minimum temperature ranges, (c) DT-AREA and DT-TEMP, (d) standardized DT-AREA and DT-TEMP, and (e) the maximum area corresponding to different minimum temperature ranges; the lines on the boxes have the same meanings as in Figure 8.

were larger than those of the QS cases but the range of variation was lower for QS. For the EP MCSs, M-AREA was larger and L-TEMP was lower, which means that the cloud shield height was higher and the convection was stronger: the inverse relationship between M-AREA and L-TEMP means that both lower L-TEMP and larger M-AREA corresponded to stronger convection.

For both MCS types, larger M-AREAs corresponded to lower L-TEMPs and L-TEMP was reached earlier than M-AREA. Compared with the QS MCSs, the M-AREAs of EP MCSs were larger and their L-TEMPs were lower, and the corresponding convection was stronger.

4. Comparison of the two-type composite circulations

The location and diurnal variation of the formation of the two MCS types were compared in Section 3, and the differences between them were related to the background circulation at formation time (Li et al., 2015; Zeng et al., 2016). The in-

terpolated CFSR reanalysis data introduced in Section 2 was used to compare the background circulations of the two MCS types and to analyze which environmental conditions were favorable for eastward propagation. The interpolated CFSR data was available at 3-h intervals. If the formation time of the MCSs corresponded to a CFSR data time, the data at that time were used. Otherwise, only cases where the difference between formation and data times was less than one hour were used. Cases where EP and QS MCSs appeared at the same time were removed from the composition. Based on these conditions, 175 EP MCSs and 480 QS cases were selected to composite the circulations.

The composite circulations at 200 hPa were similar for the two MCS types. The South Asian high controlled the regions south of 35°N. The intensity of the South Asian high for the EP MCSs was weaker than that for the QS MCSs, but the isobaric geopotential gradient was stronger, with the upper level jet (ULJ) located to the north of the study region (Figure 10a, 10b), which indicates that the steering wind at upper levels for EP MCSs was stronger. In the middle troposphere (500 hPa), differences between the circulations for the two MCS types mainly occurred at low latitudes (south of 30°N), while the circulations at middle and high latitudes were similar (Figure 10c, 10d). The EP MCSs formed in the region between the low trough east of the Tibetan Plateau (TP) and the Western Pacific Subtropical High (WPSH), but for QS MCSs, the low trough east of TP was weaker and WPSH extended westward to the study region, which was unfavorable for eastward propagation of the MCSs. At lower levels (700 hPa and 850 hPa), the background circulations and water vapor fluxes of the two MCS types were also different (Figure 11). At 700 hPa, although the southwesterly wind dominated the South China and Yangtze and Huai River regions (east of 105°E) for both types, the southwesterly wind for EP MCSs was stronger than that for QS MCSs and extended northward to the southern areas of Shandong province. For EP MCSs, the vorticity in the eastern part of the study region was stronger than that in the western part, but for QS MCSs, the vorticity in the western part was stronger. The water vapor flux for EP MCSs was stronger, and the maximum appeared in the southern part of the study region. The strong water vapor transported to east of the second-step terrain favored initiation of convection and eastward propagation of MCSs (Figure 11c). For QS MCSs, the water vapor flux was weaker and the southerly wind transported water vapor into the western part of the study region. Water vapor convergence occurred for EP MCSs in the eastern part of the study region and the Yangtze and Huai River Valley to the east of the second-step terrain (not shown), providing favorable ambient conditions for the formation and eastward propagation of MCSs.

Figure 12 shows the vertical cross section of vertical ve-

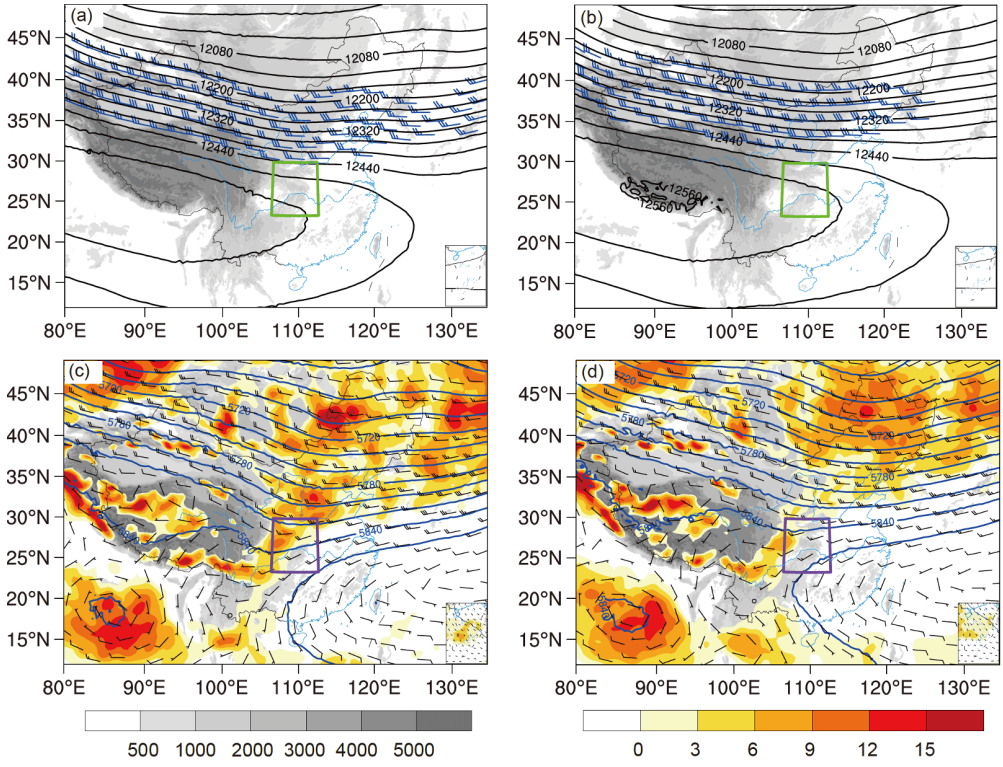

Figure 10 Composite background circulations for EP ((a), (c)) and QS ((b), (d)) MCSs at the formation stage: (a) and (b) are geopotential height (black lines, unit: gpm) and wind speeds larger than 25 m s^{-1} (wind barbs, 10 m s^{-1}) at 200 hPa; (c) and (d) are geopotential height (blue lines, unit: gpm), wind field (wind barb, 4 m s^{-1})and relative vorticity(shading, unit: 10^{-6} s^{-1}) at 500 hPa; the box denotes the study area, and gray shading denotes elevation higher than 500 m (units: m).

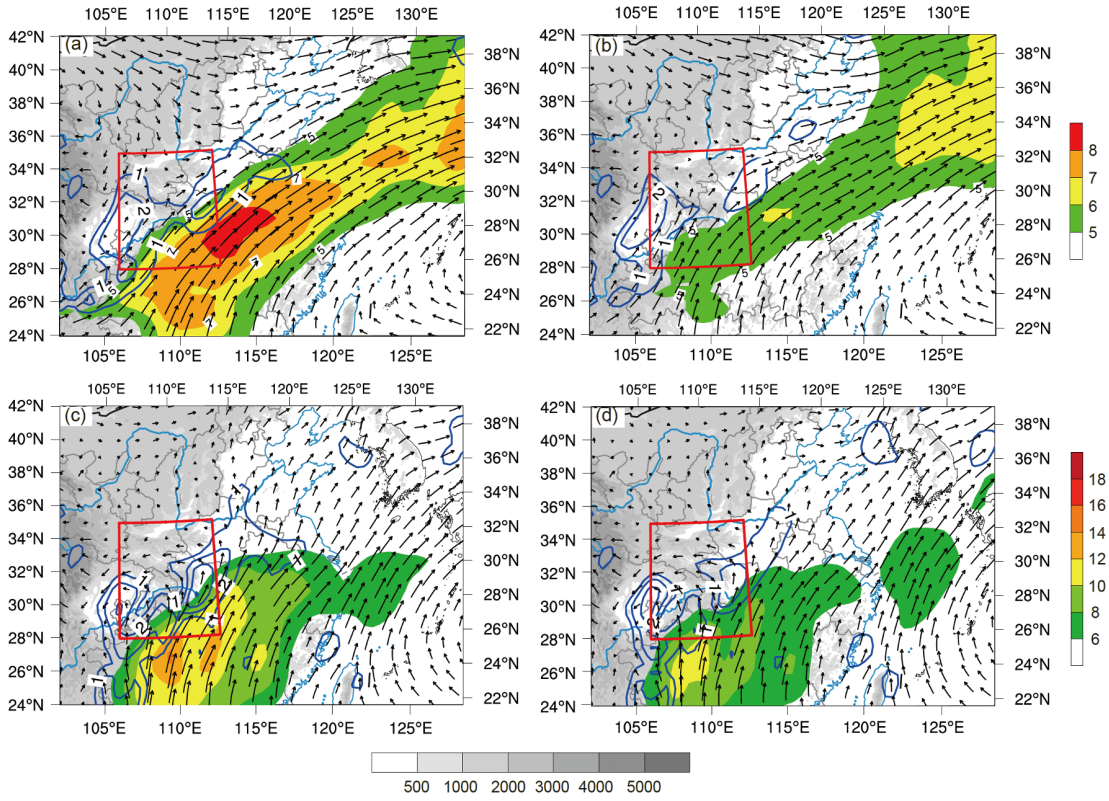

Figure 11 Composite background circulations for EP ((a), (c)) and QS ((b), (d)) MCSs at formation stage: (a) and (b) show the wind field (black vectors), wind speed (color shading, unit: m s^{-1}) and relative vorticity (blue lines, unit: 10^{-5} s^{-1}) at 700 hPa; (c) and (d) show the relative vorticity (blue line, unit: 10^{-5} s^{-1}), wind field (black vectors), and water vapor flux (color shading, unit: g s kg^{-1}) at 850 hPa. The red box denotes the MCS formation study area, and the gray shading denotes elevation higher than 500 m (units: m).

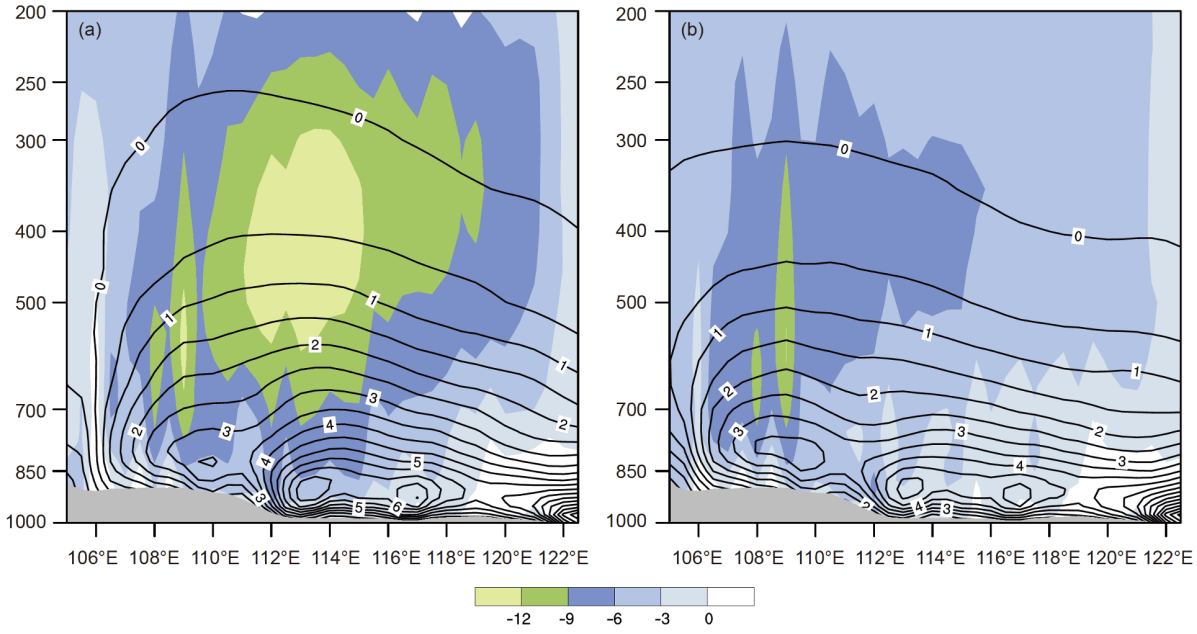

Figure 12 Height-longitudinal cross sections averaged over 28°–35°N: (a) shows EP MCSs and (b) shows QS MCSs, at formation stage. Vertical velocity is denoted by color shading (unit: Pa s^{-1}), meridional water vapor flux is denoted by black lines (unit: g s kg^{-1}) and gray shading denotes elevations averaged over 28°–35°N (units: m).

locity and meridional water vapor flux averaged over 28°–35°N for the two MCS types. Strong vertical motion occurred for QS MCSs in the western part of the study region (~109°N), between 850 hPa and 500 hPa. However, for EP

MCSs, upward motion mainly occurred in the eastern part of the study region (east of 112°E) at the middle levels of the troposphere. That was because most of the EP MCSs formed in front of the low trough over TP (Figure 10c). The largest values of meridional water vapor flux were concentrated below 700 hPa, and this flux was stronger for EP MCSs than for QS MCSs. The favorable dynamic and water vapor conditions mean that most of the EP MCSs occurred in the eastern part of the study region, with stronger convection. As well as this, positive vertical motion also appeared near 109° N for EP MCSs, which was consistent with the fact that some of these MCSs occurred in the western part of the study region.

Vertical wind shear is also an important factor for MCS evolution. Previous studies have demonstrated that the vertical wind shear has an important effect on MCS intensity and convective organization (Rotunno et al., 1988; Weisman and Rotunno, 2004; Coniglio et al., 2006; Chen et al., 2015). Vertical wind shear has a different impact on the convection at different levels, and low-level vertical wind shear directly influences convective triggering and development (Moncrieff, 1992; Xu et al., 1992; Rotunno et al., 1988; Chen et al., 2015). There was a clear 0–3 km vertical wind shear for both MCS types. For EP MCSs, strong vertical wind shear occurred from the MCS formation location to the downstream regions (Figure 13a), which further promoted the maintenance and development of convection (Bluestein and Jain, 1985; Parker and Johnson, 2000; Schumacher and Johnson, 2005; Delonge et al., 2010; Richardson et al., 2007, Zheng and Sun, 2016). The QS MCSs mainly formed in the western part of the study region, with weaker vertical motion (Figure 13b), consistent with the weaker organization and development of these MCSs.

In summary, the background circulations at middle and lower levels at the MCS formation time determined the formation location, intensity and propagation. The low trough at middle levels covering the regions from the eastern edge of TP to the eastern part of the second-step terrain, and the low-level strong vorticity, provided favorable dynamic conditions for MCS formation. The strong low-level jet provided an abundant source of water vapor for the MCS development and the westerly flow between the front of the low trough and the northwestern part of WPSH steered the MCSs eastward to the second-step terrain region downstream. Meanwhile, strong low-level wind shear favored the organization and development of EP MCSs, which were stronger and longer-lived.

5. Conclusions

A high spatial and temporal resolution TBB dataset and CFSR reanalysis data were used to recognize and track MCSs along the middle of the Yangtze River near the second-step terrain during May to August 2000–2016 (except 2005), based on an automated objective method. EP and QS MCS datasets were produced, and used to compare the spatial and temporal distribution, propagation and background circulation of these two MCS types.

A total of 193 EP MCSs and 513 QS MCSs were detected so that the eastward-propagating percentage was 27.33%. Both MCS types occurred most frequently in July. The lifetimes of EP MCSs were longer than those of QS MCSs. Most of the EP MCSs formed in the afternoon (15–18 BST), matured in the early evening to nighttime and terminated in the late evening to early morning (21–03 BST). The formation and maturity times of QS MCSs were later than those for EP MCSs, but the termination time was earlier. For both MCS types, M-AREA increased with decreasing L-TEMP, and L-TEMP was reached earlier than M-AREA. Compared with QS MCSs, it took longer for EP MCSs to reach their M-AREA and L-TEMP values. The larger M-AREA and lower

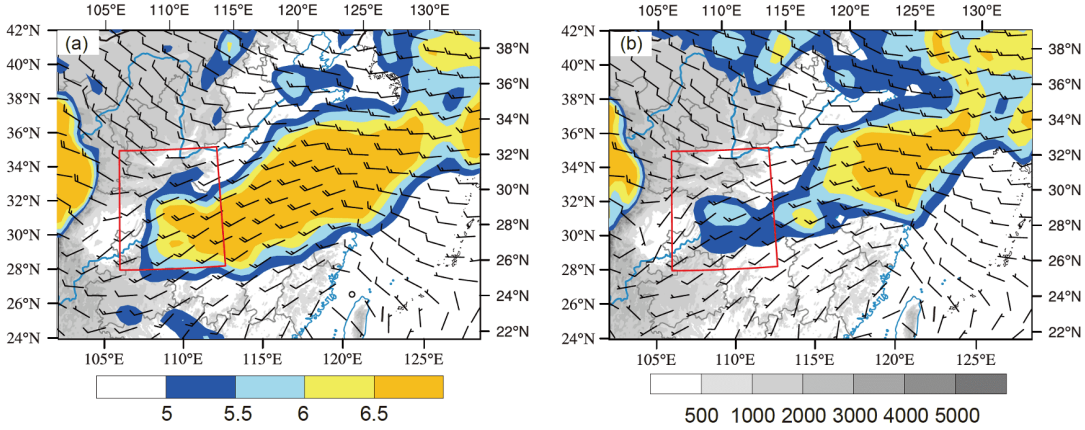

Figure 13 Composite background circulations for EP (a) and QS (b) MCSs at formation stage: 0–3 km vertical wind shear is shown as wind barbs (one bar represents 4 m s^{-1}), vertical shear wind speed is in color shading (unit: m s^{-1}), and gray shading denotes elevation higher than 500 m (units: m); the red box covers the study area.

L-TEMP of EP MCSs indicated their stronger intensity. As these MCSs propagated eastward, they influenced convection in downstream regions.

The comparison of composite background circulations at formation time demonstrated which circulations were favorable for MCS development and eastward propagation. The combination of a mid-level trough east of TP, and the WPSH, provided favorable background conditions for MCS formation and propagation. Positive vorticity over the eastern part of the second-step terrain represented favorable dynamic conditions for MCS development. A strong low-level jet transported moist and warm air to the regions east of the second-step terrain. Strong water vapor convergence, combined with strong upward vertical motion, over the eastern edge of the second-step terrain and downstream promoted the development and maintenance of convection. Meanwhile, strong vertical wind shear at middle and low levels favored the organization and evolution of MCSs and increased their lifetimes.

This study detected MCSs along the middle reaches of the Yangtze River near the second-step terrain, compared the lifetimes and background circulations of EP and QS MCSs and identified the favorable background circulations for the formation and eastward-propagation of MCSs, providing useful insights for forecasting MCSs over these regions. However, further research is needed on the mechanisms of how EP MCSs influence heavy rainfall over their downstream regions.

Acknowledgements *This research was supported by the National Key R & D Program of China (Grants No. 2018YFC1507200), and the National Natural Science Foundation of China (Grants Nos. 41505038, 91637211, 41775046 & 41575045).*

References

Ai Y F, Li W B, Meng Z Y, Li J. 2016. Life cycle characteristics of MCSs in middle east China tracked by geostationary satellite and precipitation estimates. Mon Weather Rev, 144: 2517–2530

Anderson C J, Arritt R W. 1998. Mesoscale convective complexes and persistent elongated convective systems over the United States during 1992 and 1993. Mon Weather Rev, 126: 578–599

Augustine J A, Caracena F. 1994. Lower-tropospheric precursors to nocturnal MCS development over the central United States. Weather Forecast, 9: 116–135

Augustine J A, Howard K W. 1988. Mesoscale convective complexes over the United States during 1985. Mon Weather Rev, 116: 685–701

Augustine J A, Howard K W. 1991. Mesoscale convective complexes over the United States during 1986 and 1987. Mon Weather Rev, 119: 1575–1589

Bai A J, Liu X D, Liu C H. 2011. Contrast of diurnal variations of summer precipitation between the Tibetan Plateau and Sichuan Basin (in Chinese). Plateau Meteorol, 30: 852–859

Bluestein H B, Jain M H. 1985. Formation of mesoscale lines of pirecipitation: Severe squall lines in Oklahoma during the spring. J Atmos Sci, 42: 1711–1732

Chang C H, Ding Z Y. 2015. Distribution characteristics of MCCs in eastern Tibetan Plateau in summer from 2007 to 2012 (in Chinese). J Meteorol Sci, 35: 445–453

Chen Q, Fan J, Hagos S, Gustafson Jr W I, Berg L K. 2015. Roles of wind shear at different vertical levels: Cloud system organization and properties. J Geophys Res-Atmos, 120: 6551–6574

Coniglio M C, Hwang J Y, Stensrud D J. 2010. Environmental factors in the upscale growth and longevity of MCSs derived from rapid update cycle analyses. Mon Weather Rev, 138: 3514–3539

Coniglio M C, Stensrud D J, Wicker L J. 2006. Effects of upper-level shear on the structure and maintenance of strong Quasi-Linear mesoscale convective systems. J Atmos Sci, 63: 1231–1252

Cotton W R, Lin M S, McAnelly R L, Tremback C J. 1989. A composite model of mesoscale convective complexes. Mon Weather Rev, 117: 765–783

Delonge M S, Fuentes J D, Chan S, Kucera P A, Joseph E, Gaye A T, Daouda B. 2010. Attributes of mesoscale convective systems at the land-ocean transition in Senegal during NASA African monsoon multidisciplinary analyses 2006. J Geophys Res, 115: D10213

Durkee J D, Mote T L. 2010. A climatology of warm-season mesoscale convective complexes in subtropical South America. Int J Climatol, 30: 418–431

Fu W, Wang D H, Yin H, Yin J F, Li J. 2013. Contrast analysis on statistical characteristic of MCSs over Qinghai-Xizang Plateau and East Asia in warm season (in Chinese). Plateau Meteorol, 32: 929–943

Goyens C, Lauwaet D, Schröder M, Demuzere M, Van Lipzig N P M. 2012. Tracking mesoscale convective systems in the Sahel: Relation between cloud parameters and precipitation. Int J Climatol, 32: 1921–1934

He H Z, Zhang F Q. 2010. Diurnal variations of warm-season precipitation over northern China. Mon Weather Rev, 138: 1017–1025

Hodges K I, Thorncroft C D. 1997. Distribution and statistics of African mesoscale convective weather systems based on the ISCCP Meteosat imagery. Mon Weather Rev, 125: 2821–2837

Houze R A. 2004. Mesoscale convective systems. Rev Geophys, 42: RG4003

Hu L, Deng D F, Gao S T, Xu X D. 2016. The seasonal variation of Tibetan convective systems: Satellite observation. J Geophys Res-Atmos, 121: 5512–5525

Hu M K. 1962. Visual pattern recognition by moment invariants. IEEE Trans Inform Theor, 8: 179–187

Jiang J X, Fan M Z. 2002. Convective clouds and mesoscale convective systems over the Tibetan Plateau in summer (in Chinese). Chin J Atmos Sci, 26: 263–270

Jirak I L, Cotton W R, McAnelly R L. 2003. Satellite and radar survey of mesoscale convective system development. Mon Weather Rev, 131: 2428–2449

Kidder S Q, Vonder Haar T H. 1995. Satellite Meteorology: An introduction. San Diego: Academic Press

Laing A G, Fritsch J M. 1997. The global population of mesoscale convective complexes. Q J R Met Soc, 123: 389–405

Li J. 2010. Study on the characteristics of the mesoscale convective cloud clusters occurred in East Asia during warm seasons (in Chinese). Dissertation for Doctoral Degree. Beijing: Institute of Atmospheric Physics, Chinese Academy of Sciences. 1–154

Li J Y, Shen X Y, Wang D H, Li J. 2015. Distribution and characteristics of the MCS over south China during the spring and summer of 2008 (in Chinese). J Trop Meteorol, 31: 475–485

Li J, Wang B, Wang D H. 2012. The characteristics of mesoscale convective systems (MCSs) over East Asia in warm seasons. Atmos Ocean Sci Lett, 5: 102–107

Liu R X, Ding Z Y, Sun L G,Huang H B. 2015. Statistical analysis of mesoscale convective systems over Yangtze-Huaihe basin in summer (in Chinese). Torr Rain Disast, 34: 215–222

Lu X R, Ma J, Wu C K. 1987. A Shape analytical method of two dimensional objects (in Chinese). J China Inst Commun, 8: 61–67

Maddox R A. 1980. Meoscale convective complexes. Bull Amer Meteorol Soc, 61: 1374–1387

Maddox R A. 1983. Large-scale meteorological conditions associated with midlatitude, mesoscale convective complexes. Mon Weather Rev, 111:

1475–1493
Mathon V, Laurent H. 2001. Life cycle of Sahelian mesoscale convective cloud systems. Q J R Met Soc, 127: 377–406
McAnelly R L, Cotton W R. 1992. Early growth of mesoscale convective complexes: A meso-β-scale cycle of convective precipitation? Mon Weather Rev, 120: 1851–1877
Meng Z Y, Yan D C, Zhang Y J. 2013. General features of squall lines in east China. Mon Weather Rev, 141: 1629–1647
Merritt J H, Fritsch J M. 1984. On the movement of the heavy precipitation areas of mid-latitude mesoscale convection complexes. Clearwater Beach: Conference on Weather Forecasting and Analysis. 529–536
Moncrieff M W. 1992. Organized convective systems: Archetypal dynamical models, mass and momentum flux theory, and parametrization. Q J R Met Soc, 118: 819–850
Nicolini M, Torres Brizuela M. 2002. Sensitivity of a two-dimensional convective model to turbulence parameterization. Atmósfera, 15: 193–207
Ogungbenro S B, Ajayi V O, Adefolalu D O. 2016. Mean state and kinematic properties of mesoscale convective systems over West Africa. Theor Appl Climatol, 124: 219–227
Parker M D, Johnson R H. 2000. Organizational modes of midlatitude mesoscale convective systems. Mon Weather Rev, 128: 3413–3436
Pope M, Jakob C, Reeder M J. 2008. Convective systems of the north Australian monsoon. J Clim, 21: 5091–5112
Punkka A J, Bister M. 2015. Mesoscale convective systems and their synoptic-scale environment in Finland. Weather Forecast, 30: 182–196
Qi X X, Zheng Y G. 2009. Distribution and spatiotemporal variations of deep convective over China and its vicinity during the summer of 2007 (in Chinese). J Appl Meteorol Sci, 20: 286–294
Rafati S, Karimi M. 2017. Assessment of mesoscale convective systems using IR brightness temperature in the southwest of Iran. Theor Appl Climatol, 129: 539–549
Rasmussen K L, Houze Jr R A. 2011. Orogenic convection in subtropical South America as seen by the TRMM satellite. Mon Weather Rev, 139: 2399–2420
Richardson Y P, Droegemeier K K, Davies-Jones R P. 2007. The influence of horizontal environmental variability on numerically simulated convective storms. Part I: Variations in vertical shear. Mon Weather Rev, 135: 3429–3455
Romatschke U, Houze Jr R A. 2010. Extreme summer convection in South America. J Clim, 23: 3761–3791
Rotunno R, Klemp J B, Weisman M L. 1988. A theory for strong, long-lived squall lines. J Atmos Sci, 45: 463–485
Rowell D P, Milford J R. 1993. On the generation of African squall lines. J Clim, 6: 1181–1193
Salio P, Nicolini M, Zipser E J. 2007. Mesoscale convective systems over southeastern South America and their relationship with the South American low-level jet. Mon Weather Rev, 135: 1290–1309
Schröder M, König M, Schmetz J. 2009. Deep convection observed by the Spinning Enhanced Visible and Infrared Imager on board Meteosat 8: Spatial distribution and temporal evolution over Africa in summer and winter 2006. J Geophys Res, 114: D05109
Schumacher R S, Johnson R H. 2005. Organization and environmental properties of extreme-rain-producing mesoscale convective systems. Mon Weather Rev, 133: 961–976
Sun J H, Zhang F Q. 2012. Impacts of mountain–plains solenoid on diurnal variations of rainfalls along the mei-yu front over the east China plains. Mon Weather Rev, 140: 379–397
Sun J H, Zhang X L, Qi L L, Zhang G Y, Zhao S X, Tao S Y. 2004. An analysis on MCSs in Meiyu front during 20–24 June 2002 (in Chinese). Acta Meteorol Sin, 62: 423–438
Tollerud E I, Augustine J A, Jamison B D. 1992. Cloud top characteristics of mesoscale convective systems in 1986. Atlanta: Conference on Satellite Meteorology and Oceanography. J3–J7
Tollerud E I, Collander R S. 1993. Mesoscale convective systems and extreme rainfall in the central United States. Iahs Publication. 11–11
Tomasini M, Lafore J P, Piriou C, Rock R, Ramage K, Laurent H, Morel C, Senesi S. 2006. Atlas on a climatology of West African mesoscale convective systems. AMMA European Deliverable
Trier S B, Parsons D B. 1993. Evolution of environmental conditions preceding the development of a nocturnal mesoscale convective complex. Mon Weather Rev, 121: 1078–1098
Velasco I, Fritsch J M. 1987. Mesoscale convective complexes in the Americas. J Geophys Res, 92: 9591–9613
Weisman M L, Rotunno R. 2004. "A theory for strong long-lived squall lines" revisited. J Atmos Sci, 61: 361–382
Xu K M, Arakawa A, Krueger S K. 1992. The macroscopic behavior of cumulus ensembles simulated by a cumulus ensemble model. J Atmos Sci, 49: 2402–2420
Yang X R, Fei J F, Huang X G, Cheng X P, Carvalho L M, He H R. 2015. Characteristics of mesoscale convective systems over China and its vicinity using geostationary satellite FY2. J Clim, 28: 4890–4907
Zeng B, Chen Y, Li Z C. 2016. Characteristic of precursor environment of mesoscale convective system during summer in central-eastern China (in Chinese). Plateau Meteorol, 35: 460–468
Zhang Y C, Sun J H. 2017. Comparison of the diurnal variations of precipitation east of the Tibetan Plateau among sub-periods of Meiyu season. Meteorol Atmos Phys, 129: 539–554
Zhang Y C, Zhang F Q, Davis C A, Sun J H. 2018. Diurnal evolution and structure of long-lived mesoscale convective vortices along the Mei-yu front over the East China Plains. J Atmos Sci, 75: 1005–1025
Zheng L L, Sun J H, Zhang X L, and L C H. 2013. Organizational modes of mesoscale convective systems over central East China. Weather Forecast, 28: 1081–1098
Zheng L L, Sun J H. 2013. Characteristics of synoptic and surface circulation of mesoscale convective systems in dry and moist environmental conditions (in Chinese). Chin J Atmos Sci, 37 : 891–904
Zheng L L, Sun J H. 2016. The impact of vertical wind shear on the intensity and organizational mode of mesoscale convective systems using numerical experiments (in Chinese). Chin J Atmos Sci, 40: 324–340
Zheng Y G, Chen J, Zhu P J. 2008. Climatological distribution and diurnal variation of mesoscale convective systems over China and its vicinity during summer. Chin Sci Bull, 53: 1574–1586
Zheng Y G, Xue M, Li B, Chen J, Tao Z Y. 2016. Spatial characteristics of extreme rainfall over China with hourly through 24-hour accumulation periods based on national-level hourly rain gauge data. Adv Atmos Sci, 33: 1218–1232
Zhuo H, Zhao P, Li C H, Pu Z X. 2012. Analysis of climatic characteristics of mesoscale convective system over the lower reaches of the Yellow River during summer (in Chinese). Chin J Atmos Sci, 36: 1112–1122
Zipser E J, Cecil D J, Liu C T, Nesbitt S W, Yorty D P. 2006. Where are the most intense thunderstorms on earth? Bull Amer Meteorol Soc, 87: 1057–1072

(Responsible editor: Zhiyong MENG)